JGR Space Physics

RESEARCH ARTICLE
10.1029/2022JA031275

Unraveling the Role of IMF *Bx* in Driving Geomagnetic Activity

M. V. Kubyshkina[1], V. S. Semenov[1], N. A. Tsyganenko[1], X.-G. Wang[2], and I. V. Kubyshkin[1]

[1]Department of Physics, St.Petersburg State University, St. Petersburg, Russia, [2]Department of Physics, Harbin Institute of Technology, Harbin, China

Key Points:

- AL-index dynamics is controlled by both *X* and *Y* components of interplanetary magnetic field, with and without sign dependence, respectively
- Interplanetary magnetic field (IMF) *Bx* is efficient only for nonzero values of geodipole tilt Ψ; AL-index increases/decreases if Ψ and *Bx* have the same/opposite signs
- On average, IMF *Bx* impact on AL is smaller than that of IMF *By*, except for maximum values of dipole tilt when *Bx* and *By* effects become comparable

Supporting Information:

Supporting Information may be found in the online version of this article.

Correspondence to:

M. V. Kubyshkina,
m.kubyshkina@spbu.ru

Citation:

Kubyshkina, M. V., Semenov, V. S., Tsyganenko, N. A., Wang, X.-G., & Kubyshkin, I. V. (2023). Unraveling the role of IMF *Bx* in driving geomagnetic activity. *Journal of Geophysical Research: Space Physics*, *128*, e2022JA031275. https://doi.org/10.1029/2022JA031275

Received 5 JAN 2023
Accepted 10 APR 2023

Author Contributions:

Conceptualization: M. V. Kubyshkina, V. S. Semenov, X.-G. Wang
Data curation: M. V. Kubyshkina, N. A. Tsyganenko
Formal analysis: M. V. Kubyshkina, N. A. Tsyganenko
Investigation: M. V. Kubyshkina, V. S. Semenov, I. V. Kubyshkin
Methodology: M. V. Kubyshkina
Software: M. V. Kubyshkina
Supervision: V. S. Semenov, N. A. Tsyganenko, X.-G. Wang
Validation: M. V. Kubyshkina, N. A. Tsyganenko
Visualization: I. V. Kubyshkin

Abstract In this work, we question the existing opinion that the interplanetary magnetic field (IMF) Sun-Earth (*Bx*) component is of minor importance for the geomagnetic activity and show that both *Bx* and *By*, being two principal components of the Parker's spiral, are equally important factors. We show that the asymmetric behavior of activity indices around solstices can be explained as a combination of symmetric (sign-independent) effect of IMF *By* and asymmetric (sign-dependent) effect of *Bx*, the latter interpreted as a result of the geodipole tilt influence on the magnetotail stability and nightside reconnection. We also show that, due to the 7.5° inclination of the Earth orbital plane to the solar equatorial plane, the geoeffective IMF *Bz* component may increase or decrease, depending on the IMF sector polarity and season.

Plain Language Summary Interaction of the solar wind with the Earth's magnetic field drives the magnetospheric activity and space weather. Magnetosphere's response to the external driving can be forecasted, once the incoming solar wind state and its dynamics are known. Of great importance for space weather forecasting is the interplanetary magnetic field (IMF). When its North-South component (*Bz*) turns southward, the magnetosphere energy accumulates and the geomagnetic activity increases. The other two IMF components that lie in the equatorial plane also affect the magnetosphere, but there exist different opinions on their role. In this paper we show that both Sun-Earth (*Bx*) and East-West (*By*) components are equally important. The latter component mostly affects the magnetic field dynamics on the dayside, such that its increase (regardless of orientation) enhances the activity. IMF *Bx* component affects the magnetosphere in a more complex way: its impact is small at equinoxes but increases at solstices. Due to the global spiral-shaped IMF geometry, *Bx* and *By* are strongly correlated and, hence, act simultaneously. Therefore, to evaluate the IMF impact on the magnetosphere, one should properly take into account the magnitude/orientation of all its components, combined with inclination of the Earth's dipole axis to the terminator plane.

1. Introduction

To predict the space weather and evaluate magnetic activity indices, it is common to use the coupling functions composed of interplanetary parameters. A great variety of coupling functions has been proposed in the past (e.g., Balikhin et al., 2010; Kan & Lee, 1979; McPherron et al., 2015; Newell et al., 2007; see also a detailed review by Lockwood & McWilliams, 2021). Most of them include the solar wind speed, the IMF component normal to the Sun-Earth line, $B_\perp = \sqrt{B_z^2 + B_y^2}$, and its clock angle, defined in GSM coordinates as $\theta = \tan^{-1}(|By|/Bz)$. In terms of its role in stirring up the magnetospheric activity, *Bz* component is the most important: when antiparallel to the subsolar geomagnetic field, it is the main driver of dayside reconnection. The role of *By*-component is also well established; in the commonly used coupling functions it enters in a sign-independent manner. A couple of existing additive solar wind drivers which separately treat the IMF and flow speed effects (see Boyle et al., 1997; Petrukovich, 2006), also include *By* in an even form.

By contrast, neither the *Bx*-component, nor the dipole tilt (also an important factor affecting the magnetospheric configuration) appear in the long list of coupling functions. Yet a number of studies provided convincing evidence that both *Bx* and *By* polarities play a significant role in the magnetospheric response to the solar wind driving, especially for large magnitudes of the dipole tilt angle Ψ, and their individual roles are often hard to distinguish from each other. Reistad et al. (2014) made a statistical study of global-scale features of the Earth's aurora and pointed out the importance of the IMF *Bx*-component. In particular, they concluded that the Northern/Southern hemisphere aurora are brighter for negative/positive IMF *Bx*, and explained that phenomenon by asymmetric dayside reconnection, which results in a shift of the tail plasma sheet in the North-South direction, predicted

Writing – original draft: M. V. Kubyshkina
Writing – review & editing: N. A. Tsyganenko

by Cowley (1981). Hoilijoki et al. (2014) used a global simulation and concluded that (a) a positive/negative *Bx* results in a northward/southward shift of the dayside reconnection line and (b) the field strength in the loading region is strongly affected by the IMF *Bx*.

The importance of IMF *Bx* for the substorm triggering was also confirmed by Kubyshkina et al. (2018), based on a hypothesis by Kivelson and Hughes (1990) about a smaller substorm instability threshold for a curved current sheet. At the same time, several studies proposed that the direction (sign) of the east-west (*By*) component is quite an important factor in the magnetospheric reaction to the solar wind driving. Reistad et al. (2020) showed that, once the Earth's dipole is tilted in the direction corresponding to northern winter ($\Psi < 0$), positive IMF *By* results (on average) in a larger polar cap than for negative IMF *By*, at otherwise similar conditions. Similarly, Ohma et al. (2021) showed that substorms occur more frequently when *By* and the dipole tilt Ψ have opposite signs, as compared to the case of both having the same sign (note that the *By* is in the dawn-dusk direction, while the angle Ψ is in the noon-midnight meridian plane). In a series of recent works by Holappa and Mursula (2018), Holappa et al. (2019), Holappa et al. (2020), and Holappa et al. (2021), these authors show a stronger magnetospheric response to the solar wind driving in the Northern hemisphere for $By > 0$ and $\Psi < 0$. The effect was demonstrated to manifest itself in the auroral indices (AL), precipitating energetic electron flux, and ionospheric currents. However, those authors emphasized that the IMF *Bx* was of only minor importance.

As the IMF is typically oriented along the Parker spiral, the horizontal *Bx* and *By* components are not independent and, therefore, their individual effects on the geomagnetic activity are difficult to discern from observations. In addition, the geodipole tilt was also shown to play an important role, as it severely changes the magnetospheric configuration in the noon-midnight meridian plane. In this paper, we attempt to separate *Bx* and *By* contributions and quantify the effect of the dipole tilt. We found, contrary to the findings in the above cited papers, that the *Bx* component has an independent role in driving the geomagnetic activity, and present a plausible explanation for the effect.

2. Motivation and Approach

This study was motivated by a series of papers by Holappa et al. (2020, 2019, 2021) and Holappa and Mursula (2018), in which different response of the geomagnetic activity to otherwise the same interplanetary conditions was attributed to the IMF *By*. We begin with exploring the AL-index dependence on IMF *Bx* and *By* during periods with different dipole tilt angles, using the coupling function by Newell et al. (2007) as the interplanetary driver:

$$\frac{d\Phi}{dt} = v^{\frac{4}{3}} \cdot B_{\perp}^{\frac{2}{3}} \cdot \sin\left(\frac{\theta}{2}\right)^{\frac{8}{3}},$$

where v is the solar wind speed, $B_{\perp} = \sqrt{B_y{}^2 + B_z^2}$ is the IMF transverse component, and θ is its clock angle defined as $\theta = \tan^{-1}\left(\frac{|B_y|}{B_z}\right)$. Our data source is a pool of 1-hr average OMNI data for IMF components, solar wind speed, and AL index, covering the period from 1981 to 2019.

Figure 1 shows a 38-year average distribution of AL index as a function of $d\Phi/dt$ (vertical axis) and IMF *Bx* (*By*) in panels (a) and (b), respectively. Data used in these plots correspond to 30-day intervals around winter solstices, such that the dipole tilt Ψ is negative with average value around −25°. The right panel (b) repeats the result of Holappa and Mursula (2018), showing larger AL values for positive *By*. The left panel (a) shows a very similar dependence of AL on the IMF *Bx*, namely, larger AL for $Bx < 0$. As shown below, this is due not only to the correlation between *Bx* and *By*, which questions the conclusion of Holappa and Mursula (2018) about the minor importance of the *Bx* component.

Based on only the above plots, it is impossible to uniquely determine which of the two IMF components, *Bx* or *By*, is responsible for the asymmetry of geomagnetic activity. An evident source of this ambiguity is the global spiral configuration of IMF, resulting in a close coupling of its equatorial components, such that positive *By* is associated with negative *Bx* and vice versa, provided that the IMF data are averaged over large time periods. This is illustrated in Figure 2 in the form of a scatter plot of $N = 276{,}761$ hourly values $B_{x,i}$ and $B_{y,i}$ for the whole period 1981–2019 (blue dots) and a best-fit straight line (red), based on minimizing the merit function (Press et al., 1992, Ch. 15.3)

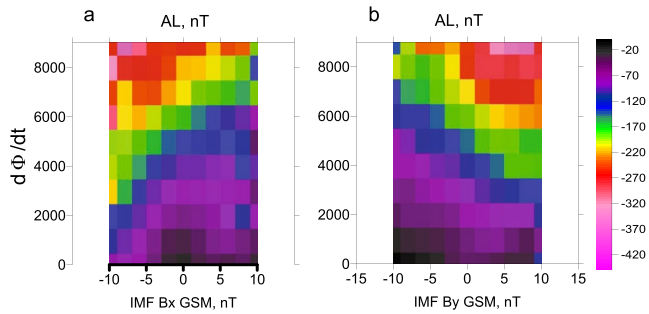

Figure 1. The AL-index dependence on the coupling function $d\Phi/dt$ and the interplanetary magnetic field (IMF) *Bx*-component (a) and the IMF *By*-component (b) near winter solstice (30 days around December 22).

$$\chi^2(a,b) = \sum_{i=1}^{N} \frac{\left[B_{y,i} - (a + bB_{x,i})\right]^2}{\sigma_{B_y}^2 + b^2\sigma_{B_x}^2},$$

where $\sigma_{B_x} = 3.67$ and $\sigma_{B_y} = 4.08$ are standard deviations of IMF B_x and B_y. Best-fit values of the intercept $a = 0.012$ and the slope $b = -1.111$ were obtained using a nonlinear search algorithm based on Nelder-Mead method (Press et al., 1992; Ch. 10.4). The Pearson correlation coefficient was found equal to $R = -0.453$. One clearly sees that the data cloud bifurcates into two symmetric regions of enhanced density in the second and fourth quadrants, due to two prevailing polarities of the IMF sectors. Note also that the obtained slope $b = -1.111$ yields the average Parker Spiral Angle PSA $= \tan^{-1}(-1.111) = 48°$, in close agreement with recent results by Chang et al. (2022), who reported that angle to lie in the range between 45° and 50° during solar min and solar max intervals, respectively.

We use henceforth the Newell et al. (2007) coupling function, but emphasize that its exact form is not critical for further analysis, since all the commonly used functions are constructed in a similar way and include the same parameters, though with different exponents. As an example, we employed a different recent coupling function by McPherron et al. (2015) in Supporting material (Figure S1a in Supporting Information S1, similar to Figure 1 format).

3. Results

Since the dependence of magnetospheric activity on the *By* polarity exists only for large values of the dipole tilt Ψ, we first checked how the influence of *Bx* and *By* on $\langle AL \rangle$ changes with variations of Ψ. Figure 3 shows the average $\langle AL \rangle$ plots (solid lines) against *Bx* (left panel) and *By* (right panel) for four intervals of Ψ. For comparison, dashed lines in the top of each panel show variations of the coupling function $\langle d\Phi/dt \rangle$ for three intervals of the tilt angle, using the same color coding.

The main features clearly evident in both plots are as follows.

1. With the $|\Psi|$ increase from 0 to 30° and $Bx = By = 0$, the $|\langle \mathrm{AL} \rangle|$ values decrease fourfold, despite the same solar wind driving. Therefore, the magnetospheric configuration changes caused by variations of the dipole tilt are quite important for the system's response to the solar wind driving.
2. For a given Ψ, the average $\langle \mathrm{AL} \rangle$ increases with growing $|By|$ and $|Bx|$. In almost a perfect match, one sees a corresponding increase in $\langle d\Phi/dt \rangle$, which is more pronounced in panel (b), as should be expected from the coupling function equation.
3. For large values of the dipole tilt, one sees an asymmetric dependence of $\langle \mathrm{AL} \rangle$ on *Bx* (smaller $|\langle \mathrm{AL} \rangle|$ for $Bx > 0$) and *By* (smaller $|\langle \mathrm{AL} \rangle|$ for $By < 0$), while the asymmetry disappears for $\Psi \sim 0$. Note that in the variations of $\langle d\Phi/dt \rangle$ the asymmetry is negligible.

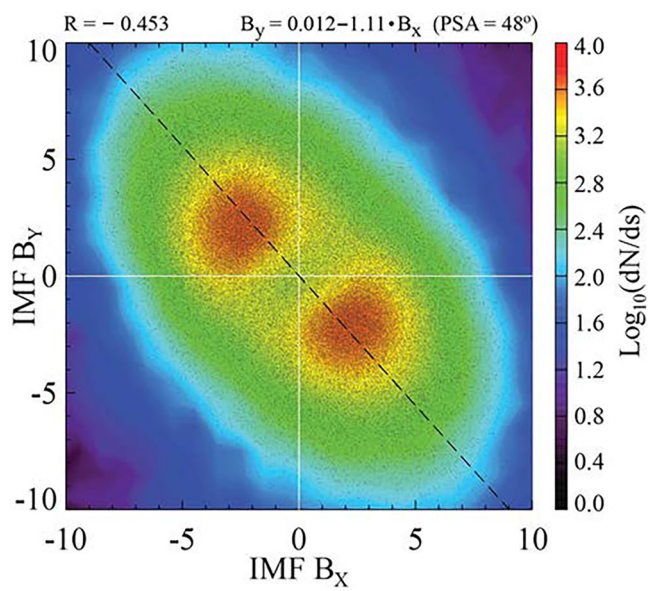

Figure 2. Scatter plot of interplanetary magnetic field (IMF) *Bx* against *By*, based on hourly OMNI data for 1981–2019. The color coding shows the logarithm of data point density per 0.1 × 0.1 nT intervals of *Bx* and *By*.

Since the asymmetric behavior of the AL index is observed only at nonzero values of the dipole tilt Ψ, we may well relate the AL dependence on *By* for $\Psi = 0$ to variations of the coupling function $\langle d\Phi/dt \rangle$. Indeed, plotting the variations of $\langle \mathrm{AL} \rangle$ against *By* and *Bx* for $\Psi = 0$ (red solid lines in Figure 3, black dots in Figure 4), we see that they are perfectly fitted by the parabola equation (red lines in Figure 4). The two fits appear very close to each other:

$$\langle \mathrm{AL}_{|\Psi=0} \rangle = -1.25 \cdot B_y^2 - 2.3 \cdot B_y - 118 \quad (1)$$

$$\langle \mathrm{AL}_{|\Psi=0} \rangle = -1.20 \cdot B_x^2 - 1.3 \cdot B_x - 119, \quad (2)$$

and their similarity suggests that they have the same cause, rooted in the coupling function dependence on *By*. That dependence is also symmetrically

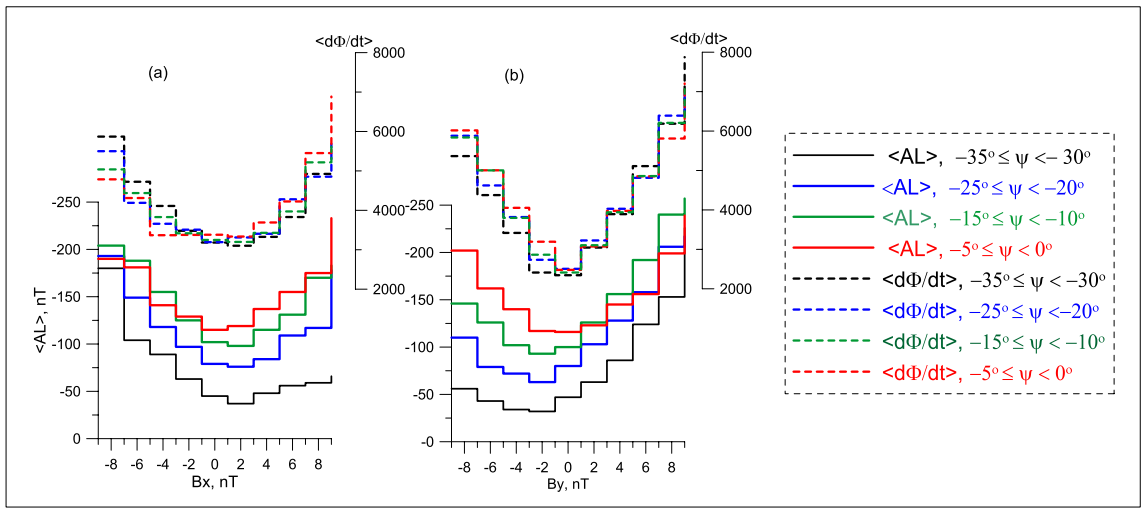

Figure 3. Average ⟨AL⟩ variation with *Bx* (left) and *By* (right) (solid lines) for four 5°-intervals of the dipole tilt Ψ. Dashed lines on top show the variation of the coupling function $\langle d\Phi/dt \rangle$ for the same intervals of Ψ.

reflected in *Bx*, because for the average spiral-shaped magnetic field line $Bx \sim -By$. Best-fit equations are given below in Figure 3 along with correlation coefficients, which are notably high in both cases: –0.96 and 0.99 for *Bx* and *By*, respectively.

Based on the above result, we subtract zero-Ψ values of ⟨AL⟩ given by Equation 2 from each of the ⟨AL⟩ versus *Bx* profiles, corresponding to consecutive intervals of the tilt Ψ (four of which are shown in the left panel of Figure 3). This straightforward procedure allows us to single out the AL-index portion that does not depend on the solar wind driver. Figure 5 shows the resulting residuals $AL_{res} = \langle AL \rangle - \langle AL \rangle|_{\Psi=0}$ for eight selected values of Ψ (plots for all Ψ intervals at 5° cadence are presented in Supporting Information S1). The values of AL_{res} are approximated by linear fits $AL_{res} = a\,Bx + c$. The correlation coefficients are greater than or equal to 0.75, except

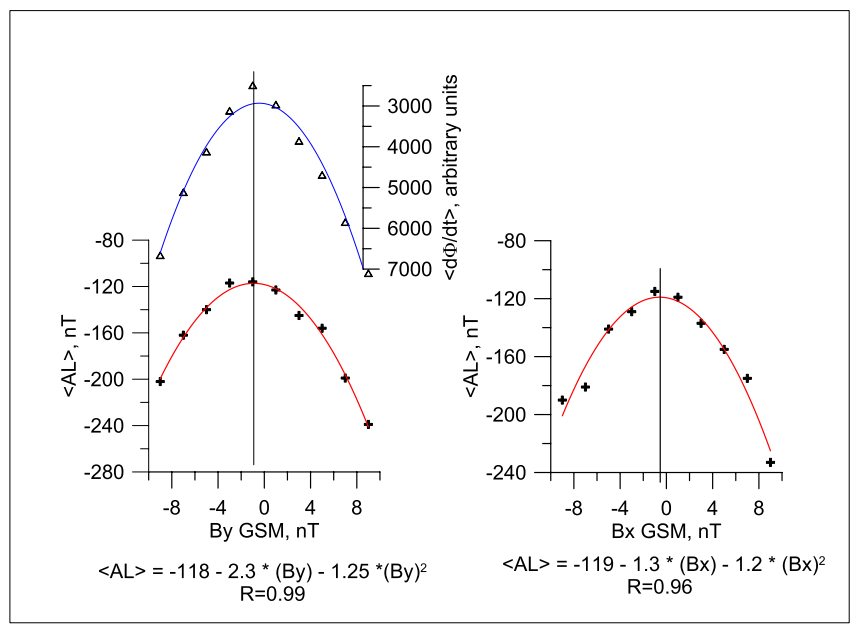

Figure 4. Parabolic fits (red lines) to the average ⟨AL⟩ dependence on *By* (left) and *Bx* (right) shown by black crosses. The black triangles and blue line in the top plot show the coupling function values and the corresponding best-fit parabola. All the plots correspond to zero dipole tilt.

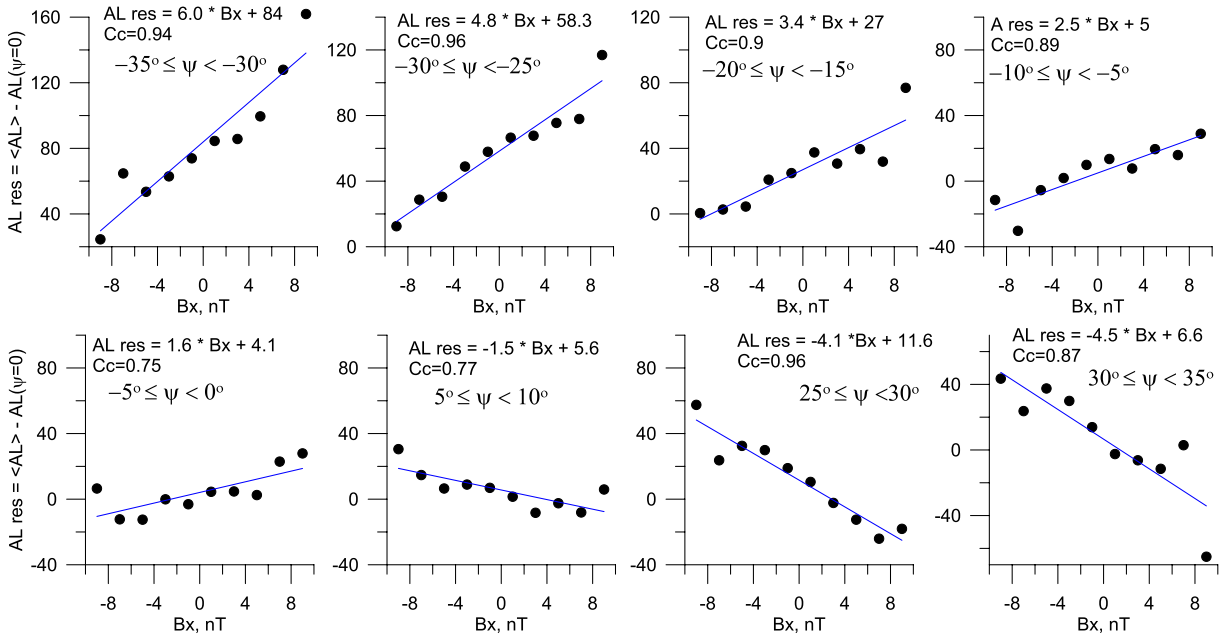

Figure 5. Residual AL_{res} (black dots), obtained by subtracting zero-tilt ⟨AL⟩ values (Equation 2), plotted against Bx for eight intervals of the dipole tilt Ψ. Best linear fits (blue) are quantified by equations on top of each plot. Correlation coefficients are given below each formula. Note the difference of vertical scales in individual panels.

in the near-zero tilt plots, where the values of AL_{res} are fourfold smaller than those for larger tilts. Regression parameters for AL_{res} corresponding to all tilt angle intervals are given in Table S1 in Supporting Information S1.

One clearly sees in Figure 5 an evident dependence of the regression coefficient "a" on the dipole tilt angle. It gradually decreases with decreasing absolute value of the tilt $|\Psi|$ and changes its sign in concert with the sign of the tilt angle Ψ. This finding is illustrated in Figure 6, showing a perfect linear correlation with a coefficient Cc = 0.97. The high correlation confirms that the observed deviations of ⟨AL⟩ from its zero-tilt value are closely related to both dipole tilt and the IMF Bx.

In regard to the free terms in the regression equations in Figure 5 (plotted in the right panel of Figure 6) one sees that the regular behavior in the winter season with large negative tilts changes to a somewhat less ordered dependence in the summer season with positive tilts (see also in Supporting Information S1). We attribute this effect to larger variations of AL index due to higher luminosity and hence larger ionization and conductivity variations during the summer period.

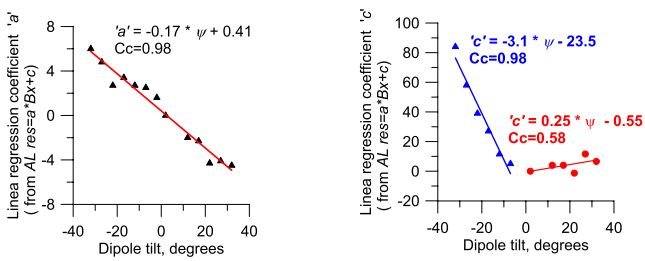

Figure 6. Regression coefficients "a" and "c" in $AL_{res} = a\,Bx + c$ against the dipole tilt, where AL_{res} is the deviation of ⟨AL⟩ from its zero-tilt reference level. Left panel—black triangles are the values of "a" taken from equations in each plot of Figure 5 (and Figure S3 in Supporting Information S1) and red line is the best fit with the equation given above. Right panel: the same for free term "c," where blue line and blue triangles corresponds to the period of negative dipole tilt, and the red line and red dots shows the "c" values during the period of positive dipole tilt.

Using the obtained regression coefficients, one may estimate the asymmetric (with respect to the driving function) part of the AL index as:

$$AL_{res} = (-0.17\,\Psi + 0.41)\cdot B_x + \begin{cases} -3.1\Psi - 23.5;\ \Psi < 0 \\ 0.25\Psi - 0.55;\ \Psi > 0 \end{cases} \quad (3)$$

Based on this result, one can represent the AL index as a sum of two terms: (a) a symmetric term, controlled by the driving function $d\Phi/dt$, independent of the By and Bx polarities, and (b) an asymmetric term AL_{res}, which depends on the dipole tilt and the signs of Bx and By.

To check if the above conjecture can be applied not only to averaged data, but also to individual data samples, we created two scatter plots of hourly AL against the symmetric driver $d\Phi/dt$: (a) using the original OMNI values and (b) using the same values, but corrected by adding the asymmetric part given by Equation 3 as AL – AL_{res}. Under assumption that the asymmetry comes

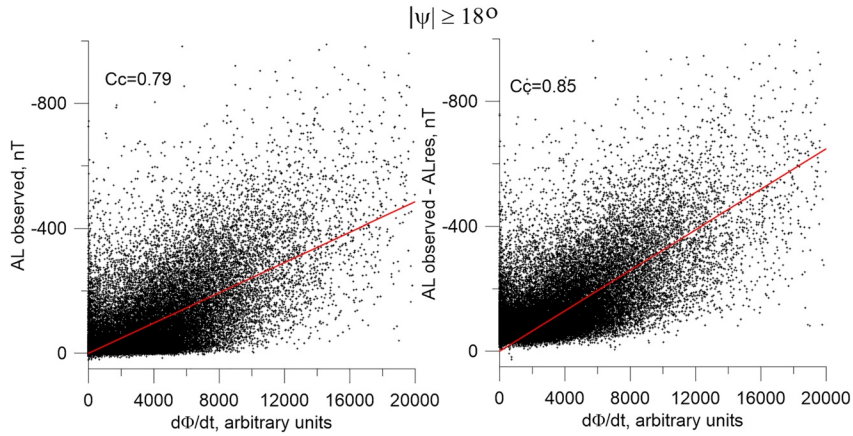

Figure 7. Left: hourly AL index against the driving function $d\Phi/dt$ during intervals with $|\Psi| > 18°$ for the period 1981–2019. Right: the same scatter plot but with added correction AL – AL_{res}, with AL_{res} calculated from Equation 3.

into effect only for large tilts, the plots were created using only data for $|\Psi| > 18°$. The result is shown in Figure 7, with a notably better correlation in the right panel.

The above results lead us to the following conclusions: (a) Large dipole tilts result in weaker average AL activity in comparison to that at small tilts. (2) An increase in IMF |*By*| (or |*Bx*|) results in larger average AL values, and this effect is symmetric with respect to *By* (and *Bx*) polarity, if the dipole tilt is close to zero. (c) Asymmetry in the AL variation due to the IMF *Bx* (or *By*) polarity shows up only at nonzero dipole tilts and increases with growing tilt. In winter seasons, positive *Bx* (negative *By*) suppresses the AL index, while negative *Bx* (positive *By*) increases AL under the same driving conditions. In summer seasons the effect is opposite (plots for the summer season are provided in Supporting Information S1). (d) Asymmetric effects are generally weaker; however, for the largest |*Ψ*| values they may become equal to IMF *By* effects.

4. Discussion

4.1. Effect of the Helioequator Inclination to the Ecliptic

In addition to the above addressed factors, there exists a relatively weak, but rather stable effect that affects the geoeffective IMF *Bz* orientation and magnitude. It is associated with the fact (sometimes overlooked) that the IMF Parker spirals, being due to the Sun's rotation, unfold not in the ecliptic (Earth's orbital) plane, but in the solar equatorial plane, tilted to the Earth's orbital plane by an angle of 7.25° (Figure 8).

As shown in the figure, Earth crosses the solar equatorial plane on December 7 and June 6 and reaches the lowest and highest heliolatitudes ±7.25° around March 7 and September 6, respectively (Meeus, 1998). In case of positive IMF sectors (*Bx*GSE > 0, *By*GSE < 0), this should result in a negative (positive) contribution to *Bz*GSE in the spring-summer (fall-winter) months. During the periods of negative IMF sectors (*Bx*GSE > 0, *By*GSE < 0) the added *Bz*GSE reverses its polarity to opposite. This effect peaks twice a year, around the times of Earth's crossing the solar equatorial plane, which by mere coincidence (defined by mutual orientation in the inertial space of the ecliptic polar axis, Earth's and Sun's rotation axes) occurs just 2 weeks before the winter and summer solstices, when the geodipole tilt reaches its extreme values.

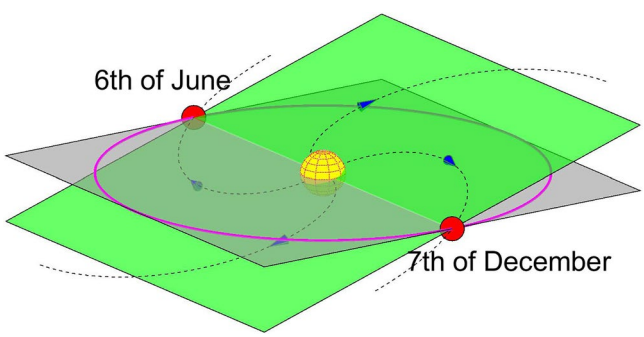

Figure 8. The tilt of the solar equatorial plane and Parker interplanetary magnetic field (IMF) spirals (green) to the Earth's orbital plane (gray). The planes intersect each other along the line, crossed by Earth twice a year, around June 6 and December 7.

The above described effect is confirmed by statistical calculations. Indeed, plotting the contours of averaged observed *Bz*GSE (OMNI data), equal intensity contours for the entire period 1981–2019 reveals a pronounced variation of *Bz*GSE with time of year and the corresponding geodipole tilt angle. This is shown in Figure 9, where left and right panels display, respectively, *Bz*GSE as a function of time (in weeks, starting from spring equinox on March 22)

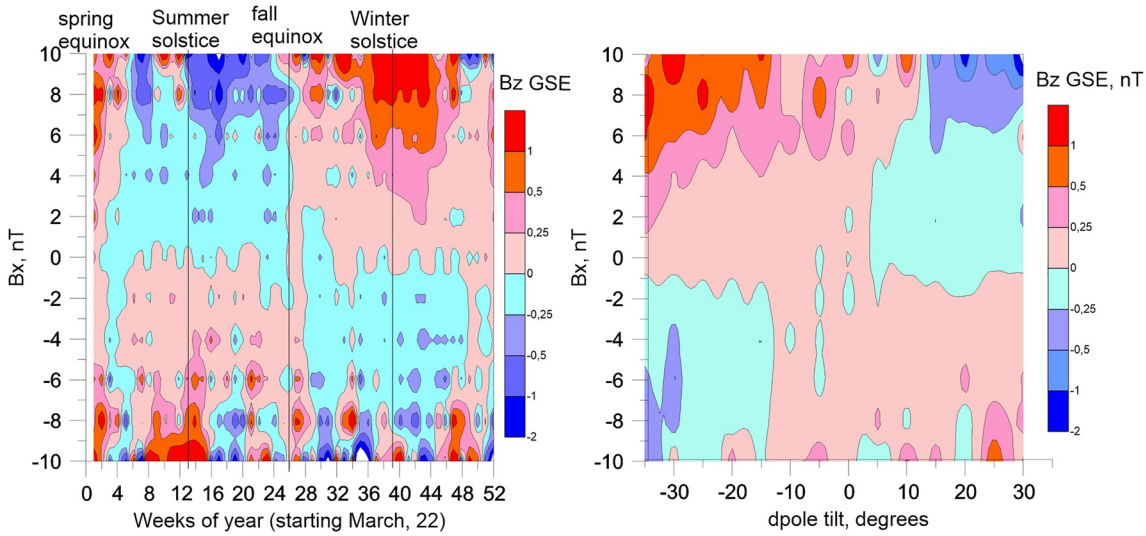

Figure 9. (Left) observed (OMNI data) average interplanetary magnetic field (IMF) *Bz*GSE distribution as a function of *Bx*GSE and of the week of year, starting from spring equinox on March 22, and (right) as a function of *Bx*GSE and the geodipole tilt angle.

and of the dipole tilt angle. One clearly sees a distinct dependence of the *Bz*GSE polarity/magnitude on the Earth's position in its orbit, as well as on the spiraling IMF direction (*Bx* polarity); we also note that the obtained alternation of the *Bz* polarity matches the obtained dependence of the magnetospheric activity on the IMF *Bx* (or *By*) polarity at large values of the geodipole tilt.

Due to the fourfold smaller variation amplitude (7.25°) of the angle between the IMF spiral plane and the ecliptic plane, the effect of the helioequator tilt is relatively small and significantly less than the well-known Russell-McPherron (1973) effect, such that typical added *Bz* is on the order of 0.5 nT.

4.2. Plasma Sheet Bending and Nightside Reconnection Threshold

The statistically significant effect of larger |AL| for smaller dipole tilts was also confirmed by Kubyshkina et al. (2015): namely, both |AL| and the lobe field intensity were found by 15%–20% larger during small dipole tilt values. Nowada et al. (2009) also reported larger |AL| for more symmetric configurations. The interpretation of these statistical results becomes transparent, if one supposes that the asymmetry of magnetospheric configurations makes the tail current sheet less stable, such that the substorm sets off under weaker driving conditions (Kivelson & Hughes, 1990). The symmetric configuration, by contrast, accumulates a larger amount of energy and causes a stronger substorm with larger |AL|. The analytical approach (Korovinsky et al., 2018), based on generalized Kan-type equilibria, also demonstrated lesser stability of the curved asymmetric magnetotail configurations.

Given this conjecture, the asymmetric dependence of AL on *Bx* (and hence *By*) at large dipole tilts can be explained by the IMF *Bx* impact on the nightside magnetospheric configuration, such that the current sheet shifts northward or southward depending on the *Bx* polarity (see Cowley, 1981 and sketches in Figure 10). If $\Psi = 0$, the *Bx*-related shift is symmetric, resulting in also symmetric dependence of AL on *Bx*. If the tilt Ψ is sufficiently large and negative (with the plasma sheet below the equatorial plane), then $Bx < 0$ moves the current sheet back toward the equatorial plane and partially restores the symmetry. By contrast, in the case $Bx > 0$ the current sheet moves further down, which increases the asymmetry. This is why no |AL| enhancement is observed for IMF $Bx > 0$ (coupled with $By < 0$), despite larger values of the coupling function. Reistad et al. (2014) suggested a similar explanation of the difference in auroral intensities in two hemispheres for different signs of IMF *Bx* (see their Figure 8).

In summary, the above presented results may be consistently explained by assuming that large tilt-related asymmetry appears due to the effect of IMF sector polarity, which (a) determines the sign of additional ΔBz due to the inclination of the solar equator to the ecliptic plane, and (b) shifts the tail current sheet from the equatorial plane.

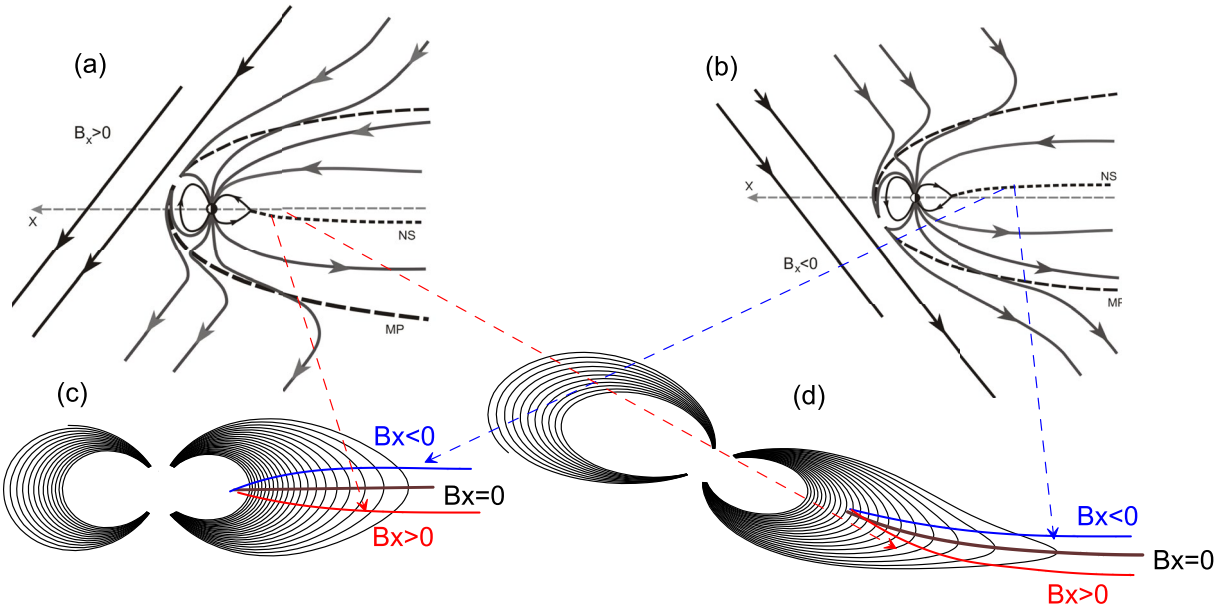

Figure 10. The asymmetric (sign-dependent) effect of interplanetary magnetic field (IMF) *Bx* on the nightside plasma sheet. Top sketches: plasma sheet displacement in the case of nonzero positive (a) and negative (b) IMF *Bx* (Cowley, 1981). Bottom: tail current sheet displacement in the case of untilted (c) and tilted (d) dipole for IMF $Bx > 0$ (red) and $Bx < 0$ (blue), the field lines for (c) and (d) are calculated using T96 model with the same input parameters. In the case $\Psi = 0$ the *Bx*-related shift is symmetric, which results in also symmetric dependence of AL on *Bx*. By contrast, at large Ψ values (here negative), the effect of *Bx* polarity is different, such that $Bx > 0$ moves the neutral sheet further down the tail and increases asymmetry, while $Bx < 0$ partially restores the symmetry.

4.3. Why Do We Question *By* as the Source of Activity Asymmetry?

The combined effect of IMF *By* and the dipole tilt on geomagnetic activity is not that obvious. Indeed, even if one takes into account the additional *By*-controlled twisting of the plasma sheet around the tail axis during winter solstices, this does not explain the persistent AL decrease for negative IMF *By*. On the other hand, the isolated (i.e., tilt-unrelated) impact of $|By|$ on the magnetospheric activity is quite clear, since the existence of nonzero *By* (regardless of its polarity) results in larger transverse component of IMF and, hence, increases the magnetic reconnection on the dayside. All the currently used solar wind–magnetosphere coupling functions reflect this by assuming even (sign-independent) variation of the magnetospheric activity with IMF $|By|$.

The above reasoning leads to a conclusion that it is the *Bx* polarity, rather than that of *By*, that results in different magnetospheric response during large dipole tilt periods.

At the same time, we admit that the proponents of *By* as a major factor (rather than *Bx*) still have a strong argument in favor of their viewpoint, based on results corresponding to periods with relatively small values of either *Bx* or *By*, as illustrated in Figures 11a and 11b. To produce those plots, we generated two subsets of data: one with $|By| < 2$ nT and the other with $|Bx| < 2$ nT. Then from the first dataset we calculated the average AL values over all $Bx > 0$ (red) and all $Bx < 0$ (blue) for different levels of Newell's driving function $d\Phi/dt$. Panel (b) displays similar plots, but averaged over $By > 0$ and $By < 0$. As can be seen in the upper plots, the distance between the blue and red curves in panel (b) is larger than that in panel (a). Note that both $\langle AL \rangle$ curves were calculated here in a similar way as in Holappa and Mursula (2018) for AL and by Reistad et al. (2020) for the size of auroral oval.

One might argue that the larger separation of the curves in Figure 11b than that in Figure 11a is a signature of predominant importance of the *By* polarity. However, examination of the statistics of the IMF components included in the datasets shows that the first subset with small $|Bx|$ includes data with much larger *By* range than the range of *Bx* in the second subset with small $|By|$ (see Figure 11c with green and pink histograms for *By* and *Bx*, respectively). The existence and relative abundance of large *Bx* and *By* values is an important factor, affecting the magnitude variation of the activity index. We attribute the larger separation of the curves in Figure 11b to the different distributions of the IMF component magnitudes in the data subsets. Also, it is worth mentioning that both data subsets are inherently composed of statistically unlikely events (see Figure 2).

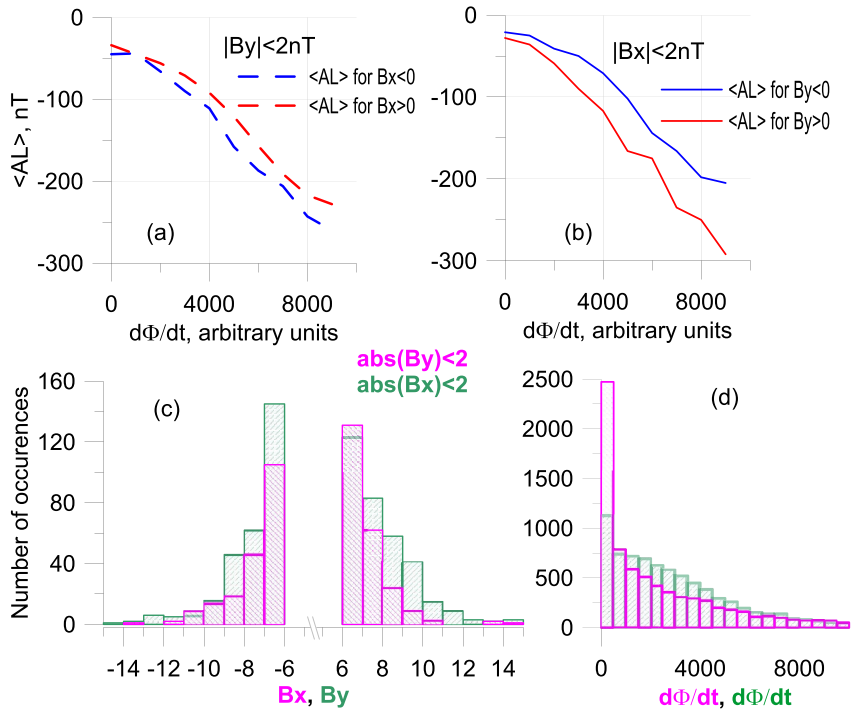

Figure 11. (a) Difference in ⟨AL⟩, averaged over all $Bx > 0$ (red dashed line) and over all $Bx < 0$ (blue dashed line) in a dataset with $|By| < 2$ nT. (b) The same for $By > 0$ and $By < 0$ in a dataset with $|Bx| < 2$ nT. (c and d) Histograms of Bx and By (left) and of the Newell's coupling function $d\Phi/dt$ (right), for the datasets with small $|By| < 2$ nT (magenta) and small $|Bx| < 2$ nT (green).

Based on the above, we conclude that the IMF Bx component is a more likely reason for the asymmetric response of the magnetosphere to the interplanetary driving during large dipole tilts, even though the close correlation between Bx and By in the Parker spiral still prevents an unambiguous interpretation. Our conclusion in favor of the Bx component follows mostly from the geometric argument, based on the current sheet transverse motion away from the equatorial plane caused by the changing dipole tilt, enhanced or weakened by the superposed IMF Bx. The combined effect of these two factors allows one to consistently explain the observed behavior of activity variations.

5. Conclusions

In this paper we provided a description and explanation of the observed response of the averaged AL-index to variations of the dipole tilt and IMF Bx and By components, with the following results:

1. The magnetospheric asymmetry due to the dipole tilt affects the nightside reconnection: the tail current sheet becomes less stable at large $|\Psi|$, such that the instability sets off earlier in the loading process, or as a result of a weaker driving (i.e., smaller loaded energy). This is why the average observed AL is smaller (up to four times) at large tilts. Symmetric configurations (at small tilts) are more stable, they store larger magnetic fluxes and lead to less frequent but stronger disturbances, manifested in larger AL values.
2. IMF Bx increases or decreases the magnetospheric asymmetry by moving the tail current sheet away from its average position, affecting its stability and, hence, the average disturbance level. More specifically:
   - The IMF Bx effect shows up only during periods with nonzero dipole tilt Ψ and acts asymmetrically, depending on the signs of both Bx and Ψ. If the signs are the same (opposite), then AL increases (decreases).
   - On the average, the effect of Bx is smaller than that of By; it maximizes during maximum $|\Psi|$ periods (when it becomes comparable to that of By) and almost disappears for $\Psi = 0$.
3. The IMF Parker spirals unfold themselves in the solar equatorial plane, which is inclined by the angle 7.25° to the ecliptic plane. In case of a positive sector (i.e., IMF away from Sun, or BxGSE < 0), this results in

additional negative *Bz* peaking around December 7 and additional positive *Bz* that peaks around June 6. For IMF sectors with positive *Bx*GSE (IMF toward the Sun), the effect in *Bz* has the opposite polarity.

4. The observed variations of ⟨AL⟩ with the IMF *Bx* and *By* during different seasons can be explained by two simultaneous effects: the symmetric (sign independent) effect of *By* on the dayside magnetopause reconnection and asymmetric (sign dependent) effect of *Bx* on the tail current sheet stability and nightside reconnection. But one has to keep in mind that on the average, *Bx* and *By* components are strongly coupled in the spiral configurations of IMF and, hence, act simultaneously. This is why their effects are hard to distinguish in statistical studies.

Though we analyzed only the AL-index behavior, our findings may be transferred to other manifestations of geomagnetic activity, such as those addressed in studies that followed the work by Holappa and Mursula (2018), for example, Holappa et al. (2019), Holappa et al. (2020), Reistad et al. (2020), Ohma et al. (2021), and Holappa et al. (2021). In those papers, statistical dependence on the *By* polarity was revealed for a wide range of activity parameters: the potential drop across the polar cap, electron precipitating flux, the size of auroral oval, substorm probability, etc. As an example, we included Figure S5 in Supporting Information S1, showing a Polar Cap index for the northern hemisphere, produced in the same manner as Figure 1 in this main paper. Another example is Figure S1b in Supporting Information S1 with substorm probability dependence on *Bx* and on a solar wind driver, obtained from data on energetic electron injections near geosynchronous orbit from Borovsky and Yakymenko (2017).

Data Availability Statement

The IMF components, solar wind data, the AL and PC indices were downloaded from the low resolution OMNI2 database http://omniweb.gsfc.nasa.gov. Substorm list based on injections of energetic electrons is available in Supporting Information S1 to the paper by Borovsky and Yakymenko (2017): https://agupubs.onlinelibrary.wiley.com/action/downloadSupplement?doi=10.1002%2F2016JA023625&file=jgra53356-sup-0001-TextS1.txt. All datasets used to obtain the above described results are available for downloading from Zenodo repository, see https://dx.doi.org10.5281/zenodo.7827612.

Acknowledgments
This work was supported by the Russian Science Foundation Grant 23-47-00084 "Magnetic Reconnection in Space and Laboratory Plasmas: Computer Simulations and Empirical Modeling" and the NSFC Grant #42261134533.

References

Balikhin, M. A., Boynton, R. J., Billings, S. A., Gedalin, M., Ganushkina, N., Coca, D., & Wei, H. (2010). Data based quest for solar wind-magnetosphere coupling function. *Geophysical Research Letters*, *37*(24), L24107. https://doi.org/10.1029/2010GL045733

Borovsky, J. E., & Yakymenko, K. (2017). Substorm occurrence rates, substorm recurrence times, and solar wind structure. *Journal of Geophysical Research: Space Physics*, *122*(3), 2973–2998. https://doi.org/10.1002/2016JA023625

Boyle, C. B., Reiff, P. H., & Hairston, M. R. (1997). Empirical polar cap potentials. *Journal of Geophysical Research*, *102*(A1), 111–125. https://doi.org/10.1029/96JA01742

Chang, Q., Xu, X., Wang, X., Ye, Y., Xu, Q., Wang, J., et al. (2022). The solar wind Parker spiral angle distributions and variations at 1 AU. *The Astrophysical Journal*, *931*(2), 105. https://doi.org/10.3847/1538-4357/ac6bf3

Cowley, S. W. H. (1981). Asymmetry effects associated with the x-component of the IMF in a magnetically open magnetosphere. *Planetary and Space Science*, *29*(8), 809–818. https://doi.org/10.1016/0032-0633(81)90071-4

Hoilijoki, S., Souza, V. M., Walsh, B. M., Janhunen, P., & Palmroth, M. (2014). Magnetopause reconnection and energy conversion as influenced by the dipole tilt and the IMF Bx. *Journal of Geophysical Research: Space Physics*, *119*(6), 4484–4494. https://doi.org/10.1002/2013JA019693

Holappa, L., Asikainen, T., & Mursula, K. (2020). Explicit IMF By-dependence in geomagnetic activity: Modulation of precipitating electrons. *Geophysical Research Letters*, *47*(4), e2019GL086676. https://doi.org/10.1029/2019GL086676

Holappa, L., Gopalswamy, N., & Mursula, K. (2019). Explicit IMF By-effect maximizes at subauroral latitudes (dedicated to the memory of Eigil Friis-Christensen). *Journal of Geophysical Research: Space Physics*, *124*, 2854–2863. https://doi.org/10.1029/2018JA026285

Holappa, L., & Mursula, K. (2018). Explicit IMF by dependence in high-latitude geomagnetic activity. *Journal of Geophysical Research: Space Physics*, *123*(6), 4728–4740. https://doi.org/10.1029/2018JA025517

Holappa, L., Robinson, R. M., Pulkkinen, A., Asikainen, T., & Mursula, K. (2021). Explicit IMF By-dependence in geomagnetic activity: Quantifying ionospheric electrodynamics. *Journal of Geophysical Research: Space Physics*, *126*(4), e2021JA029202. https://doi.org/10.1029/2021JA029202

Kan, J. R., & Lee, L. C. (1979). Energy coupling function and solar wind-magnetosphere dynamo. *Geophysical Research Letters*, *6*(7), 577–580. https://doi.org/10.1029/GL006i007p00577

Kivelson, M. G., & Hughes, W. J. (1990). On the threshold for triggering substorms. *Planetary and Space Science*, *38*(2), 211–220. https://doi.org/10.1016/0032-0633(90)90085-5

Korovinskiy, D. B., Kubyshkina, D. I., Semenov, V. S., Kubyshkina, M. V., Erkaev, N. V., & Kiehas, S. A. (2018). On application of asymmetric Kan-like exact equilibria to the Earth magnetotail modeling. *Annales Geophysicae*, *36*(2), 641–653. https://doi.org/10.5194/angeo-36-641-2018

Kubyshkina, M., Tsyganenko, N., Semenov, V., Kubyshkina, D., Partamies, N., & Gordeev, E. (2015). Further evidence for the role of magnetotail current shape in substorm initiation. *Earth Planets and Space*, *67*(1), 139. https://doi.org/10.1186/s40623-015-0304-1

Lockwood, M., & McWilliams, K. A. (2021). On optimum solar wind-magnetosphere coupling functions for transpolar voltage and planetary geomagnetic activity. *Journal of Geophysical Research: Space Physics*, *126*(12), e2021JA029946. https://doi.org/10.1029/2021JA029946

McPherron, R. L., Hsu, T.-S., & Chu, X. (2015). An optimum solar wind coupling function for the AL index. *Journal of Geophysical Research: Space Physics*, *120*(4), 2494–2515. https://doi.org/10.1002/2014JA020619

Meuss, J. (1998). *Astronomical algorithms*, 2nd ed. Willmann-Bell Inc.

Newell, P. T., Sotirelis, T., Liou, K., Meng, C.-I., & Rich, F. J. (2007). A nearly universal solar wind-magnetosphere coupling function inferred from 10 magnetospheric state variables. *Journal of Geophysical Research*, *112*(A1), A01206. https://doi.org/10.1029/2006JA012015

Nowada, M., Shue, J.-H., & Russell, C. T. (2009). Effects of dipole tilt angle on geomagnetic activity. *Planetary and Space Science*, *57*(11), 1254–1259. https://doi.org/10.1016/j.pss.2009.04.007

Ohma, A., Reistad, J. P., & Hatch, S. M. (2021). Modulation of magnetospheric substorm frequency: Dipole tilt and IMF by effects. *Journal of Geophysical Research: Space Physics*, *126*(3), e2020JA028856. https://doi.org/10.1029/2020JA028856

Petrukovich, A. A. (2006). Solar wind density effect on the night-side geomagnetic activity (AL index). *Journal of Atmospheric and Solar-Terrestrial Physics*, *68*(16), 1843–1849. https://doi.org/10.1016/j.jastp.2006.07.004

Press, W. H., Teukolsky, S. A., Vetterling, W. T., & Flannery, B. P. (1992). *Numerical recipes in FORTRAN* (2nd ed.). University Press.

Reistad, J. P., Laundal, K. M., Ohma, A., Moretto, T., & Milan, S. E. (2020). An explicit IMF By dependence on solar wind-magnetosphere coupling. *Geophysical Research Letters*, *47*(1), e2019GL086062. https://doi.org/10.1029/2019GL086062

Reistad, J. P., Østgaard, N., Laundal, K. M., Haaland, S., Tenfjord, P., Snekvik, K., et al. (2014). Intensity asymmetries in the dusk sector of the poleward auroral oval due to IMF Bx. *Journal of Geophysical Research: Space Physics*, *119*(12), 9497–9507. https://doi.org/10.1002/2014JA020216

Russell, C. T., & McPherron, R. L. (1973). Semiannual variation of geomagnetic activity. *Journal of Geophysical Research*, *78*(1), 92–108. https://doi.org/10.1029/JA078i001p00092